New Journal of Physics
The open access journal at the forefront of physics

Deutsche Physikalische Gesellschaft DPG IOP Institute of Physics

PAPER • OPEN ACCESS

Temporal characterization of a multi-wavelength Brillouin–erbium fiber laser

New Journal of Physics
The open access journal at the forefront of physics

Deutsche Physikalische Gesellschaft DPG
IOP Institute of Physics

Published in partnership with: Deutsche Physikalische Gesellschaft and the Institute of Physics

OPEN ACCESS

RECEIVED
24 September 2015

REVISED
7 March 2016

ACCEPTED FOR PUBLICATION
13 April 2016

PUBLISHED
6 May 2016

PAPER

Temporal characterization of a multi-wavelength Brillouin–erbium fiber laser

Victor Lambin Iezzi[1,2], Thomas F S Büttner[1], Amirhossein Tehranchi[3], Sébastien Loranger[2], Irina V Kabakova[1,4], Benjamin J Eggleton[1] and Raman Kashyap[2,3]

[1] Centre for Ultrahigh bandwidth Devices for Optical Systems (CUDOS), Institute of Photonics and Optical Science (IPOS), School of Physics, University of Sydney, NSW, 2006, Australia
[2] Department of Physics Engineering, Polytechnique Montréal, 2900 Édouard-Montpetit, Qc, Montreal H3T 1J4, Canada
[3] Department of Electrical Engineering, PolyGrames, Polytechnique Montréal, 2900 Édouard-Montpetit, Qc, Montreal H3T 1J4, Canada
[4] Blackett Laboratory, Imperial College London, London SW7 2AZ, UK

E-mail: victor.lambin-iezzi@polymtl.ca

Keywords: Brillouin scattering, multi-wavelength laser, Brillouin eribum laser, fiber laser

Abstract

This paper provides the first detailed temporal characterization of a multi-wavelength-Brillouin–erbium fiber laser (MWBEFL) by measuring the optical intensity of the individual frequency channels with high temporal resolution. It is found that the power in each channel is highly unstable due to the excitation of several cavity modes for typical conditions of operation. Also provided is the real-time measurements of the MWBEFL output power for two configurations that were previously reported to emit phase-locked picosecond pulse trains, concluded from their autocorrelation measurements. Real-time measurements reveal a high degree of instability without the formation of a stable pulse train. Finally, we model the MWBEFL using coupled wave equations describing the evolution of the Brillouin pump, Stokes and acoustic waves in the presence of stimulated Brillouin scattering, and the optical Kerr effect. A good qualitative consistency between the simulation and experimental results is evident, in which the interference signal at the output shows strong instability as well as the chaotic behavior due to the dynamics of participating pump and Stokes waves.

1. Introduction

Multi-wavelength sources with a constant channel spacing that is in the order of tens of gigahertz are useful for many applications such as metrology [1], spectroscopy [2], arbitrary waveform generation [3], microwave synthesizers [4], wavelength division multiplexing (WDM) [5, 6] and high-speed optical clocks [7] for optical communications. Among other techniques [8–10], Brillouin-based lasers have gained considerable attention due to their advantages such as their simplicity, robustness, and only need for standard components. Stimulated Brillouin scattering (SBS) is a third order coherent interaction between a pump wave, an acoustic wave and a red-shifted Stokes wave [11]. In silica optical fibers, it can be used to generate new optical frequency components that are shifted by ~10 GHz without the need for high speed electronics. Multi-wavelength sources based on cascaded SBS (cSBS) have been demonstrated in different configurations such as short Fabry–Perot fiber resonators [3, 12] on-chip waveguide [13], whispering-gallery mode resonators [4] and hybrid Brillouin–erbium ring lasers [14–19]. Others have also used forward SBS in microstructured fibers [20].

Hybrid multi-wavelength Brillouin and erbium fiber lasers (MWBEFLs) have been widely investigated as they are particularly interesting because of their low power threshold [21], large tunability [5, 16, 22] and ability to generate many Brillouin shifted frequencies [23, 24]. Their basic principle is to combine the narrow nonlinear gain offered by SBS in an undoped fiber with the broadband linear gain from an erbium doped fiber to enable the cascaded processes of SBS. Several configurations have been studied including self-starting [14], Raman [25, 26] or Rayleigh assisted [17, 23], all of which show very similar spectral characteristics. MWBEFLs have often been suggested to be useful sources for optical communication [5, 7, 22, 24], in particular for WDM systems.

MWBEFLs have been characterized by measuring their optical and radio frequency (RF) spectra [27, 28]. Long term temporal stability on the time scale of minutes has been demonstrated by performing consecutive measurements of the optical spectrum [5, 15, 24, 29, 30]. Recently, autocorrelation measurements of MWBEFLs have been presented that indicated the generation of pulses in the time domain and phase-locking of the Stokes waves was suggested [31]. However, despite numerous demonstrations of different configurations of MWBEFLs, these lasers have not been characterized in the time domain with sufficiently high resolution. Since MWBEFLs rely on relatively long resonators, several longitudinal resonator modes lie under the Brillouin gain curve in each frequency channel. Excitation of modes and gain competition between these modes, as well as mode detuning and the presence of weak external feedback could lead to temporal instabilities [32, 33]. The demonstration of stable continuous-wave operation of the frequency channels spaced by ~10 GHz is thus required in order to confirm the usefulness of an MWBEFL for telecommunications.

In this paper, we temporally characterize two MWBEFL configurations with two different types of fibers of different lengths. The output intensity of the MWBEFL is measured on pico- to micro-second time scales. The waveforms resulting from the interference of the different frequency channels as well as the intensity of the individual frequency channels are recorded in real-time. Real-time measurements of configurations that were previously reported to emit picosecond pulse trains based on autocorrelation measurements are also further characterized temporally. For the MWBEFL configurations investigated here, excitation of several cavity modes in each frequency channel is observed in the regime of cSBS. Finally, we present a model which governs the propagation of pump, Stokes and acoustic waves consisting of coupled wave equations for cSBS, Kerr nonlinearities and include random mode hopping. We use the simulation to explain the experimental results of the MWBEFL, by finding instability in the temporal evolution of output pulses as well as participating pump and Stokes waves. This instability for typical conditions of operation represents a fundamental issue for MWBEFL configurations with long resonators for which the solution cannot be easily addressed by using feedback mechanisms such as electronic locking to compensate for environmental fluctuations.

2. Experimental setup

Two different MWBEFL configurations, namely single-cavity and dual-cavity, are investigated as shown in figures 1(a) and (b), respectively. In both configurations, comb-like spectra are generated by cSBS. In both configurations the same variables can be tuned: the Brillouin pump (BP) that seeds the SBS process and the intra-cavity gain provided by the EDFA. In the single-cavity configuration (figure 1(a)), even and odd orders of Stokes waves co-propagate in the cavity due to the presence of a reflector. The BP power injected into the input coupler was tuned between 0.25 and 1.5 W as EDFA #1 could deliver up to 2 W. Similar powers were needed while comparing single and dual cavity configuration. However, higher BP power was needed for the shorter highly nonlinear silica fiber (HNLF) than for the longer single-mode fiber (SMF)-28 fiber. This leads to a channel spacing of the out-coupled light of $\nu_B \sim 10.85$ GHz, the Brillouin frequency shift of the fiber at 1550 nm. In the dual-cavity configuration (figure 1(b)), even and odd orders of Stokes waves propagate in opposite directions leading to a channel spacing of twice the Brillouin frequency shift ($2\nu_B \sim 21.70$ GHz). For each configuration, temporal characterizations are performed using a few kilometers long (~2.5 km) of SMF-28 similar to the configuration reported in [31]. Furthermore, both configurations are characterized using a shorter length (~135 m) of HNLF as proposed in [27]. This fiber has a smaller core compared to SMF-28, and therefore exhibits better mode confinement and an increased effective nonlinearity ($\gamma \sim 21\ \mathrm{km}^{-1}\ \mathrm{W}^{-1}$). The HNLF zero dispersion wavelength is at 1551 nm.

To characterize each configuration, pump light from a single frequency DFB laser, which is further amplified with EDFA #1, is coupled into the resonator through a 95:5 coupler. Inside the resonator, gain is provided by an in-cavity EDFA #2 in order to reduce the threshold for cSBS generation. Once the gain is higher than the loss in the resonator, the first Stokes wave is generated. Subsequently, this first Stokes wave acts as a pump for a second Stokes wave and so on, leading to higher-order Stokes waves generation. Even and odd Stokes waves circulate in the same direction in the first configuration due to the reflection at the gold-tipped fiber mirror, whilst they circulate in opposite directions in the dual-cavity configuration using two circulators to separate the directions. A 3 nm band-pass filter prevents self-lasing cavity modes in an undesired spectral region [16]. A 99:1 coupler is used to collect the output power for characterization. The output power was typically about a few mW at the output coupler.

The characterization of the individual lines (section 3.1) is performed by directing the optical output spectrum to a wave-shaper (filter) with a minimum filter bandwidth of 10 GHz (~0.078 nm at around 1550 nm) and then separating it into individual channels, which are detected by three identical fast photodiodes. These signals are then simultaneously observed on a 64 GHz real-time oscilloscope. The output light is spectrally characterized (results in section 3.2) with an optical spectrum analyzer with a 0.1 pm resolution. The autocorrelation trace is also measured via an FR-103XL autocorrelator and real-time acquisition is performed with a 50 GHz photodiode and a 64 GHz oscilloscope. The measurement instruments are shown in detection part of figure 1(c).

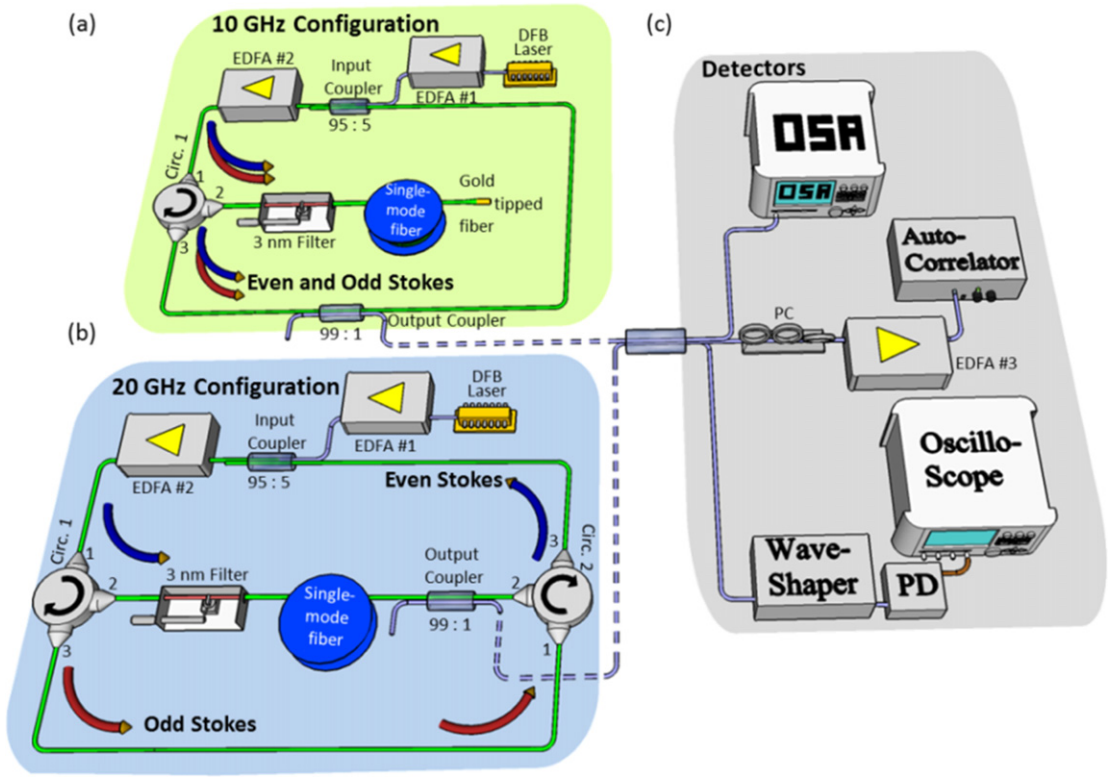

Figure 1. Experimental setup of a (a) single-cavity configuration combining all Stokes waves in one direction generating a frequency comb with a spacing of ~10.85 GHz. (b) Even and odd Stokes waves are separated in the dual-cavity configuration leading to a frequency comb generation with a spacing of ~20.70 GHz. (c) Detection part including an optical spectrum analyzer (OSA) to acquire the frequency comb, an autocorrelator following an EDFA and a polarization controller (PC) to observe the autocorrelation function of the pulses and a wave-shaper combined with a photodiode (PD) and a real-time oscilloscope to resolve temporally the output power.

3. Experimental results

3.1. Individual line characterization

In order to determine the usefulness of the described MWBEFL configurations as stable multi-wavelength sources, we first characterize the temporal performance of individual frequency channels, corresponding to the different orders of Stokes waves.

The first set of measurements is related to the spectral and temporal characterization of the pump and Stokes lines of MWBEFLs using a 135 m long HNLF. The optical spectrum is shown in figure 2(a), depicting the BP, *P* and two main Stokes lines, namely the second Stokes wave, *S*2 and the fourth Stokes wave, *S*4. In figure 2(b), we present a real-time measurement of the power fluctuations of the three lines (*P*, *S*2 and *S*4) filtered separately from the output of the dual-cavity configuration.

The pump and two Stokes waves at the output shown in figure 2(b) exhibit strong intensity fluctuation, even though the pump has a very narrow linewidth and is temporally stable at the input. The insets in figure 2(b) corresponds to one roundtrip of the pump and even-order Stokes waves. Strong power fluctuations can be observed well below the roundtrip time on a timescale of ~10 ns. Similar results can be observed for a single-cavity configuration, however due to the limitation of the wave-shaper filtering (bandwidth >10 GHz), the individual frequency channels were not sufficiently isolated in this case. The individual line characterization of the dual-cavity configuration is shown with a 135 m long HNLF, however similar characteristics are observed using a 2.5 km long of SMF-28. In the case of the long resonator (2.5 km, FSR = ~80 kHz), there are 250 modes within a Stokes linewidth while for the short resonator (135 m (~165 m with connecting fibers and in-cavity EDFA), FSR = ~1.2 MHz), approximately 17 modes exist under each Stokes linewidth. Figure 2(c) shows a fast Fourier transform (FFT) performed on the temporal data of a filtered channel (second Stokes in this case). The beating of the resonator modes at harmonics of 1.2 MHz, corresponding to the FSR of the cavity, can be seen in figure 2(c). It is important to note here that this system may be stable during a small time span. Indeed, during our experiments, some rare measurements showed stable single-mode operation for few tens of μs. However, those measurements were not reproducible and

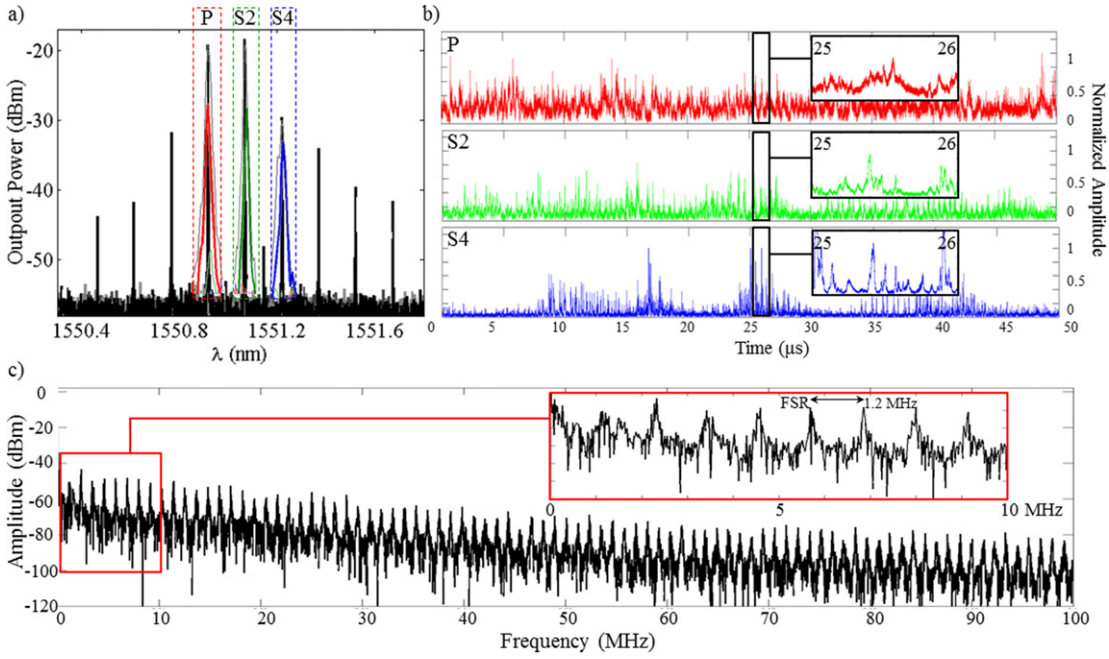

Figure 2. (a) Output optical spectrum from a dual-cavity MWBEFL using a 135 m of HNLF giving a channel spacing of 0.15 nm. The colored insets represent the zoomed Stokes spectrum after the wave-shaper narrowband filter (the width of each channel has been amplified for visual purposes), (b) simultaneous temporal characterizations of three waves taken individually over a span of 50 μs show considerable fluctuations. Insets show power fluctuation over a cavity roundtrip. (c) Fast Fourier transform performed on a filtered channel (the second Stokes: S2) shown on a frequency span of 100 MHz. Cavity modes are clearly seen in the inset, spaced by 1.2 MHz corresponding to the free spectral range (FSR) of the ~135 m cavity (~165 m with connecting fibers and in-cavity EDFA).

extremely rare. Therefore, the measurement shown here is a common case in which a stable period of a few μs can be observed.

3.2. Multi-Stokes characterization

In the second set of measurements we temporally characterized the MWBEFL without using spectral filters. Two examples of the measured output spectra are shown in figure 3(a), for single- and dual-cavity systems using a 2.5 km long SMF-28. Several lines are formed by the pump, Stokes waves and anti-Stokes waves where the latter is generated via four wave mixing (FWM). Corresponding autocorrelation measurements are shown in figure 3(b) for both systems matching well what was reported in [31] showing a relatively large autocorrelation background. The peak spacing of 46 ps for the dual-cavity system corresponds to 21.7 GHz, thus twice the Brillouin frequency shift, while a spacing of 92 ps for the single-cavity system correspond to the Brillouin frequency shift of an SMF-28, i.e. 10.85 GHz. The total spectral width of this laser leads to a time width of the autocorrelation peak of roughly 15 ps at the autocorrelator for both configurations as they have similar total spectral width.

Figure 3(c) shows a real-time oscilloscope measurement of the dual-cavity configuration over a time window of 50 μs (~4 roundtrips) with a temporal resolution limited by the instrument to ~15 ps. Similar interference signals are observed with the single-cavity configuration, but to avoid redundancy only the results of the dual-cavity one are shown. We observed strong fluctuations of the envelope of the beat signal of pump and Stokes waves on the order of 10 ns. We attribute these fluctuations to the excitation of many resonator modes under the Brillouin gain curves. This is even more obvious in a close-up taken over a time window of 5 μs as shown in figure 3(d). The insets in figure 3(d) depict 0.5 ns zoomed-in sections showing interference signals centered at three different times, from the same MWBEFL. The insets illustrate how the waveform of the output light changes on a timescale well below the roundtrip time.

Figures 3(e) and (f) show the FFT of the temporal data of the dual-cavity and single-cavity configuration with a frequency spacing of 21.7 and 10.85 GHz respectively. Many resonator modes under each Stokes bandwidth were observed, as can be seen in the 100 MHz zoomed-in sections in both figures 3(e) and (f). Even though figure 3(e) depicts the result for the dual-cavity one, a residual beat note at ~10.85 GHz can be observed. Here, we have shown the results of both MWBEFL configurations with a 2.5 km fiber spool as an example.

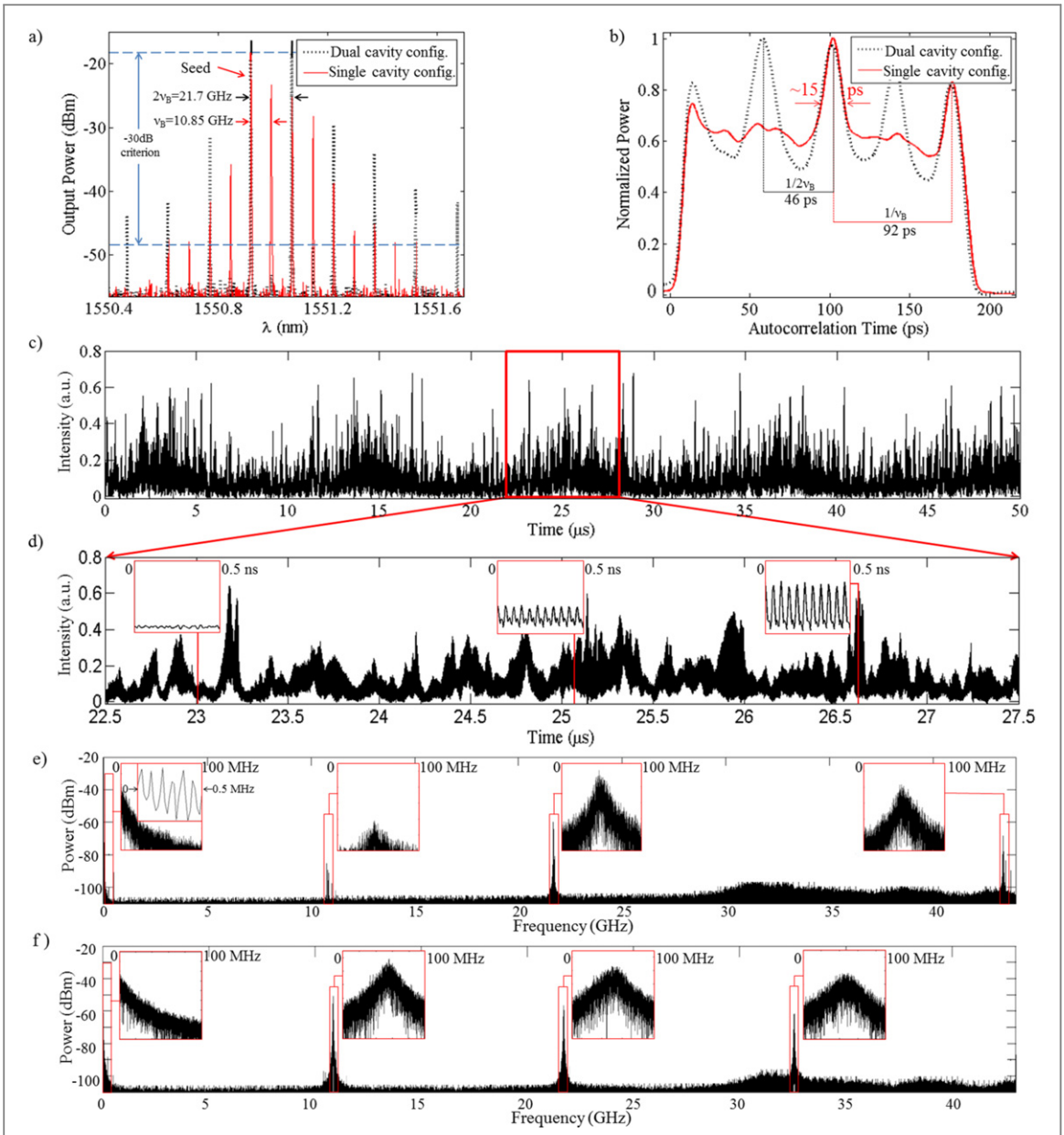

Figure 3. (a) Typical frequency comb output spectra from a single-cavity (red solid line) and dual-cavity (black dotted line) MWBEFL for a 2.5 km long SMF-28 with a frequency spacing of 10.85 GHz and 21.7 GHz, respectively. (b) Autocorrelation measurement at the same output port showing some pulse-like generation. (c) Real-time oscilloscope measurement for the dual-cavity MWBEFL showing low degree of coherence over a 50 μs time span. (d) 5 μs zoomed-in section from (c) with three 0.5 ns time-window insets showing interference signals centered at three different times. (e) FFT of the temporal signal data collected in the dual-cavity MWBEFL output. Insets are 100 MHz-wide zoomed-in spectra centered at 50 MHz, 10.85 GHz, 21.70 GHz and 43.40 GHz respectively from left to right. The 500 kHz spectral close-up on the most left inset shows cavity modes spaced by ~80 kHz equal to the FSR of the cavity. (f) FFT performed on the temporal signal data at the single-cavity MWBEFL output. Insets are 100 MHz-wide zoomed-in spectra centered at centered at 50, 10.85, 21.70 and 32.55 GHz from left to right.

Nevertheless, similar observations remain with a 135 m long HNLF instead since in this configuration many cavity modes also lie under the Brillouin gain curves.

4. Theoretical model and numerical analysis

To get a deeper insight on the evolution of Stokes lines using the cSBS in the resonator and to explain the experimental results, we propose a model to numerically simulate the pump and Stokes waves dynamics in a dual-cavity MWBEFL. The simulated resonator corresponds to the one shown in figure 1(b). In the model, we included forward and backward propagating pump and higher order Stokes waves. Dispersion has been neglected in this model. The dispersion length for the considered bandwidth (bandwidth for ~20 ps pulses) is tens of kilometers, and therefore for short cavities of 135 m HNLF, dispersion is negligible. For longer cavities of

2.5 km SMF-28, dispersion might have a small effect after several roundtrips, however we can assume that such effects will only be detrimental to the mode, phase and pulse stability. Therefore, neglecting dispersion as a best-case scenario, considering the generation of Stokes waves up to the 4th-order, we have the following coupled equations among the Stokes and pump wave considering SBS, and the optical Kerr effect [12, 34, 35]

$$\frac{1}{\nu}\frac{\partial E_p^{\pm}}{\partial t} \pm \frac{\partial E_p^{\pm}}{\partial z} = -\frac{ng_B}{4\eta_0}E_{s1}^{\mp}Q_1^{\pm} - \frac{\alpha}{2}E_p^{\pm} + in_2k_0(2E_{s1}^{\pm}E_{s2}^{\pm}E_{s3}^{\pm *} + 2E_{s1}^{\pm}E_{s3}^{\pm}E_{s4}^{\pm *} + E_{s1}^{\pm}E_{s1}^{\pm}E_{s2}^{\pm *} + E_{s2}^{\pm}E_{s2}^{\pm}E_{s4}^{\pm *}) + in_2k_0(2\,|E_T|^2 - |E_p^{\pm}|^2)E_p^{\pm}, \quad (1)$$

$$\frac{1}{\nu}\frac{\partial E_{s1}^{\pm}}{\partial t} \pm \frac{\partial E_{s1}^{\pm}}{\partial z} = +\frac{ng_B}{4\eta_0}(E_p^{\mp}Q_1^{\mp *} - E_{s2}^{\mp}Q_2^{\pm}) - \frac{\alpha}{2}E_{s1}^{\pm} + in_2k_0(2E_p^{\pm}E_{s3}^{\pm}E_{s2}^{\pm *} + 2E_{s2}^{\pm}E_{s3}^{\pm}E_{s4}^{\pm *} + 2E_p^{\pm}E_{s4}^{\pm}E_{s3}^{\pm *} + 2E_p^{\pm}E_{s2}^{\pm}E_{s1}^{\pm *} + E_{s2}^{\pm}E_{s2}^{\pm}E_{s3}^{\pm *}) + in_2k_0(2\,|E_T|^2 - |E_{s1}^{\pm}|^2)E_{s1}^{\pm}, \quad (2)$$

$$\frac{1}{\nu}\frac{\partial E_{s2}^{\pm}}{\partial t} \pm \frac{\partial E_{s2}^{\pm}}{\partial z} = +\frac{ng_B}{4\eta_0}(E_{s1}^{\pm}Q_2^{\pm *} - E_{s3}^{\pm}Q_3^{\mp}) - \frac{\alpha}{2}E_{s2}^{\pm} + in_2k_0(2E_p^{\pm}E_{s3}^{\pm}E_{s1}^{\pm *} + 2E_{s1}^{\pm}E_{s4}^{\pm}E_{s3}^{\pm *} + 2E_{s1}^{\pm}E_{s3}^{\pm}E_{s2}^{\pm *} + E_{s1}^{\pm}E_{s1}^{\pm}E_p^{\pm *} + E_{s3}^{\pm}E_{s3}^{\pm}E_{s4}^{\pm *} + 2E_p^{\pm}E_{s4}^{\pm}E_{s3}^{\pm *}) + in_2k_0\times(2\,|E_T|^2 - |E_{s2}^{\pm}|^2)E_{s2}^{\pm}, \quad (3)$$

$$\frac{1}{\nu}\frac{\partial E_{s3}^{\pm}}{\partial t} \pm \frac{\partial E_{s3}^{\pm}}{\partial z} = +\frac{ng_B}{4\eta_0}(E_{s2}^{\pm}Q_3^{\pm *} - E_{s4}^{\pm}Q_4^{\mp}) - \frac{\alpha}{2}E_{s3}^{\pm} + in_2k_0(2E_{s1}^{\pm}E_{s2}^{\pm}E_p^{\pm *} + 2E_{s1}^{\pm}E_{s4}^{\pm}E_{s2}^{\pm *} + 2E_p^{\pm}E_{s4}^{\pm}E_{s1}^{\pm *} + 2E_{s2}^{\pm}E_{s4}^{\pm}E_{s3}^{\pm *} + E_{s2}^{\pm}E_{s2}^{\pm}E_{s1}^{\pm *}) + in_2k_0(2\,|E_T|^2 - |E_{s3}^{\pm}|^2)E_{s3}^{\pm}, \quad (4)$$

$$\frac{1}{\nu}\frac{\partial E_{s4}^{\pm}}{\partial t} \pm \frac{\partial E_{s4}^{\pm}}{\partial z} = +\frac{ng_B}{4\eta_0}E_{s3}^{\mp}Q_4^{\mp *} - \frac{\alpha}{2}E_{s4}^{\pm} + in_2k_0(2E_{s2}^{\pm}E_{s3}^{\pm}E_{s1}^{\pm *} + 2E_{s1}^{\pm}E_{s3}^{\pm}E_p^{\pm *} + E_{s3}^{\pm}E_{s3}^{\pm}E_{s2}^{\pm *} + E_{s2}^{\pm}E_{s2}^{\pm}E_p^{\pm *}) + in_2k_0(2\,|E_T|^2 - |E_{s4}^{\pm}|^2)E_{s4}^{\pm}, \quad (5)$$

$$\frac{\partial Q_1^{\pm}}{\partial t} = \frac{1}{\tau_a}\left(-Q_1^{\pm} + E_p^{\pm}E_{s1}^{\mp *} + i\frac{f}{g_2}\right), \quad (6)$$

$$\frac{\partial Q_2^{\pm}}{\partial t} = \frac{1}{\tau_a}\left(-Q_2^{\pm} + E_{s1}^{\pm}E_{s2}^{\mp *} + i\frac{f}{g_2}\right), \quad (7)$$

$$\frac{\partial Q_3^{\pm}}{\partial t} = \frac{1}{\tau_a}\left(-Q_3^{\pm} + E_{s2}^{\pm}E_{s3}^{\mp *} + i\frac{f}{g_2}\right), \quad (8)$$

$$\frac{\partial Q_4^{\pm}}{\partial t} = \frac{1}{\tau_a}\left(-Q_4^{\pm} + E_{s3}^{\pm}E_{s4}^{\mp *} + i\frac{f}{g_2}\right), \quad (9)$$

where $E_j^{\pm} = \sqrt{P_j^{\pm}\,2\eta_0/(nA_{\text{eff}})}$ and $P_j^{\pm}$ are the amplitudes and powers of the pump ($j = p$) and of the Stokes waves ($j = s1$, $s2$, $s3$ and $s4$), respectively. $Q_q^{\pm}$ ($q = 1,\ 2,\ 3$ and 4) are the amplitudes of the acoustic waves of the qth-order. The superscripts $\pm$ represent the direction of propagation and $|E_T|^2 = \sum_\delta |E_\delta^{\pm}|^2$, ($\delta = p$, $s1$, $s2$, $s3$ and $s4$). τ_a is the damping time of acoustic waves (phonon lifetime). n and n_2 are the linear and nonlinear refractive indexes of the fiber and $k_0 = 2\pi/\lambda_p$. Also, g_B, α and A_{eff} are the Brillouin gain coefficient, attenuation coefficient and effective core area of the fiber. $\eta_0 = 1/(c\varepsilon_0)$ is the free-space wave impedance where ε_0 the permittivity and c is the speed of light. $\nu = c/n$ is the light velocity in the fiber. f is the Langevin noise source describing the thermal fluctuations in the density of fiber resulting in spontaneous Brillouin scattering [36]. $g_2 = \pi n^5 p_{12}\varepsilon_0/(\lambda_p \nu_a)$ is the photon–phonon coupling coefficient and p_{12} is the longitudinal photo-elastic constant of the fiber and ν_a is the sound velocity in the fiber. The BP and generated Stokes lines are then amplified by the in-cavity EDFA. To model the amplifier, the equations describing the evolution of the erbium-doped fiber amplifier pump, and signals (BP and Stokes lines) are used [37].

We can evaluate the evolutions of the optical waves propagating through the components in the dual-cavity configuration of figure 1(b) during several round-trips. In each counter clock-wise round trip in the upper ring, the amplified narrow-linewidth BP light with the amplitude $E_{BP} = \sqrt{P_{BP}\,2\eta_0/(nA_{\text{eff}})}$, and Stokes waves (seeded by noise) pass through the input coupler, amplified by the in-cavity EDFA (#2) and attenuated by the circulator

and filter loss, to reach the fiber-spool's input end. The evolution of these forward (+) propagating waves all together with backward (−) propagating waves in the fiber-spool length are then solved using the coupled equations. The backward propagating waves, obtain different linear phase shifts by traveling in the cavity and are attenuated by the filter, two circulators and the coupler. The attenuated forward propagating waves then are added to the BP wave from the input coupler, amplified by the in-cavity EDFA (#2) and attenuated by the circulator and filter before reaching the fiber spool. This provides the new propagating waves for the next iteration. The boundary conditions for the pump wave and Stokes waves ($j = s1, s2, s3$ and $s4$), can be written as:

$$E_p^{+\,(m)}(0, t) = [E_p^{+\,(m-1)}(L, t)\mathrm{e}^{-\mathrm{i}\varphi_p}\alpha_{\mathrm{cir2}}\sqrt{\kappa_2}\sqrt{\kappa_1} + E_{\mathrm{BP}}(\mathrm{i}\sqrt{1-\kappa_1})]G^{(m)}\alpha_{\mathrm{cir1}}\alpha_{\mathrm{Fil}}, \tag{10}$$

$$E_j^{+\,(m)}(0, t) = [E_j^{+\,(m-1)}(L, t)\mathrm{e}^{-\mathrm{i}\varphi_j}\alpha_{\mathrm{cir2}}\sqrt{\kappa_2}\sqrt{\kappa_1}]G^{(m)}\alpha_{\mathrm{cir1}}\alpha_{\mathrm{Fil}}, \tag{11}$$

$$E_p^{-(m)}(L, t) = E_p^{-(m-1)}(0, t)\mathrm{e}^{-\mathrm{i}\varphi_p}\sqrt{\kappa_2}\alpha_{\mathrm{cir1}}\alpha_{\mathrm{cir2}}\alpha_{\mathrm{Fil}}, \tag{12}$$

$$E_j^{-(m)}(L, t) = E_j^{-(m-1)}(0, t)\mathrm{e}^{-\mathrm{i}\varphi_j}\sqrt{\kappa_2}\alpha_{\mathrm{cir1}}\alpha_{\mathrm{cir2}}\alpha_{\mathrm{Fil}}, \tag{13}$$

where m is the round-trip counter, $G^{(m)}$ is the amplitude gain in each trip, α_{cir} and α_{Fil} are the amplitude loss of the circulator and filter, and κ_1 and κ_2 are the power ratio of the input and output couplers, respectively. φ_p and φ_j are the total linear phase accumulated by the pump and Stokes waves per round trip, respectively. Existence of several longitudinal modes beneath the Brillouin gain bandwidth has been approximated as having a single mode within each SBS bandwidth, which changes to another mode randomly within the SBS bandwidth at each roundtrip. Each mode of each Stokes changes independently from one to another within its corresponding SBS bandwidth, giving a random frequency differential between each Stokes, which corresponds statistically, to the SBS bandwidth.

With the aforementioned model, we examine the dynamics of the BP and Stokes lines of the MWBEFL considering the generation of Stokes up to the 4th order, using equations (1)–(9), resulting in 18-coupled equations and numerically solve them repeatedly (as the round trips continue) by the method of characteristics [38]. For this purpose, we consider the partial differential equations as a set of ordinary differential equations involving only time derivatives by transforming the variables to the frames moving with the pump and each Stokes wave, i.e., along the characteristics $z - \nu t$ and $z + \nu t$. Then, the equations are solved using the standard Runge–Kutta method. The BP power is assumed as a CW wave at 1550.9 nm, amplified and partially launched into a resonator including a single-mode HNLF/SMF-28 fiber spool with a length of 135/2500 m, a linear refractive index of ~1.45, a nonlinear refractive index of $\sim 5 \times 10^{-20}$ m^2 W^{-1}, a fiber loss coefficient of 0.5/0.2 dB km^{-1}, effective mode area of 10/80 μm^2, a Brillouin gain coefficient of $\sim 2.5 \times 10^{-11}$ m W^{-1}, a photo-elastic constant of ~0.286, phonon life time of ~10 ns and an acoustic velocity of ~5960 m s^{-1}. For this length of fiber, the transit time trip through the HNLF/fiber is ~0.7/12 μs.

To better understand the dynamics of the BP and Stokes of the MWBEFL including HNLF, we simulate the evolutions of optical amplitudes propagating in the laser cavity during several transit times, t_{T}. Figure 4(a) depicts the power variation of the pump, 2nd and 4th Stokes waves at the output coupler in a time span of $100t_{\mathrm{T}}$ (equal to ~70 μs) for similar experimental condition of figure 2 where the BP and Stokes dynamics show strong instability. Similar to the experimental result shown in figure 2(b), the simulation qualitatively demonstrates chaotic operation of the resonator where the generation of 4th-order Stokes appears less frequently over time compared to the 2nd-order Stokes, and stops randomly for a few t_{T} (equal to a few μs). It is important to note that the knowledge of the phases of the waves is critical for an exact simulation. As this is virtually impossible to get, the comparison simply demonstrates the chaotic nature of the process, with features that change dramatically with the smallest change applied to the phase, due to the several round-trip and long lengths involved. FFT performed on a Stokes ($S2$) wave is shown on a frequency span of 100 MHz in figure 4(b) where cavity modes are clearly seen, spaced by ~1.4 MHz corresponding to the FSR of the ~135 m cavity. FFT of the calculated temporal signal data at the output is shown in figure 4(c) where the pump, second and fourth Stokes waves with many modes beneath them are noticeable. The lower noise in this FFT compared to experimental results can be explained by the fact that simulation does not take into account environment fluctuations (thermal, strain) which affect phase along the long cavity and add more noise.

In the next step, the dynamics of the amplitude at the output of the dual-cavity MWBEFL including a 2.5 km long SMF-28 is simulated. Figure 5(a) illustrates the envelope of the interference signal versus time (for $4t_{\mathrm{T}}$ equal to ~50 μs) using similar experimental condition of figure 3(a). The envelope is modulated, and thus is not constant in time due to the random changes in the phase relationship of the participating BP and Stokes waves. Figure 5(b) depicts the zoomed-in area in figure 5(a) over $0.4t_{\mathrm{T}}$, equal to ~5 μs proving that the output power of

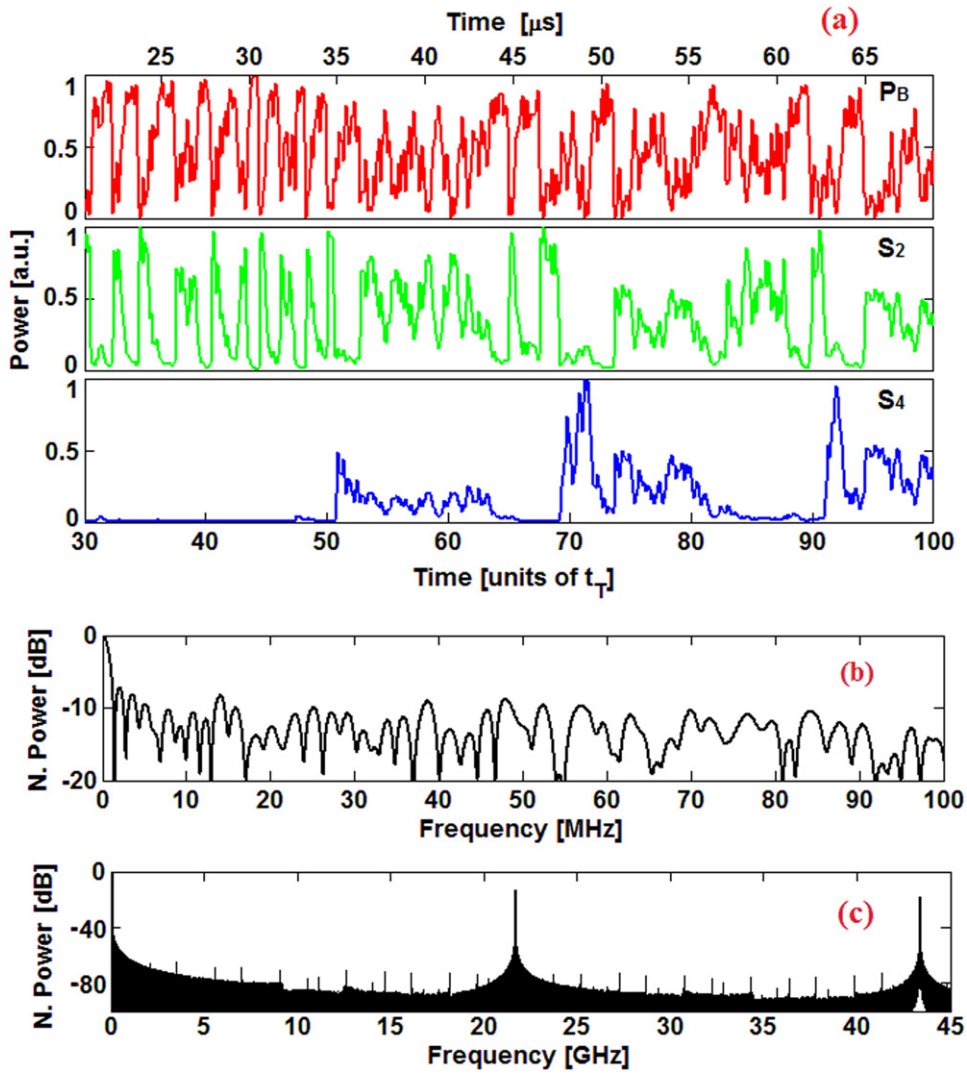

Figure 4. (a) Computed temporal evolution of the BP, second and fourth Stokes power over 100 t_T, equal to 70 μs at the output of the dual-cavity configuration including a 135 m long HNLF spool. (b) FFT performed on a Stokes (*S2*) signal shown on a frequency span of 100 MHz where cavity modes are clearly seen. (c) FFT of the calculated temporal signal data at the output where the pump, second and fourth Stokes waves are visible.

the MWBEFL is unstable in the time scale of sub-microsecond. The insets in (b) show interference signal powers centered at two different times in two 0.5 ns time-windows. These confirm the ~15 ps generated pulse trains however, a second frequency at $2 \times 2\nu_B \sim 43.4$ GHz as a result of interference between the BP and the fourth-order Stokes wave is apparent. These disclose differences in pulse profile as a result of different interferences between the BP and the higher-order Stokes wave (with different powers and phases).

5. Discussion

Temporal characterizations of the individual BP, second- and fourth-order Stokes waves and the interference signal at the output of the MWBEFLs were performed both experimentally and theoretically and a good qualitative consistency between the measurement and simulation is found. Contrary to a single-Stokes emission laser [39, 40] where the modes can be locked under some conditions, a cascaded MWBEFL exhibits a constant instability. From our theoretical study, we believe this is due to an interaction between each Stokes where power is continuously transferred thus creating out-of-phase modes. The beating of such modes brings a chaotic variation in the amplitude over time. The results shown here clearly indicate that when an MWBEFL is used with a long closed cavity (including more than one longitudinal mode within a Stokes linewidth), chaotic SBS dynamics occur, initiated by the different modes with different phases and powers, making such a source highly unstable in intensity over time. We believe that those strong power fluctuations on a time scale below the

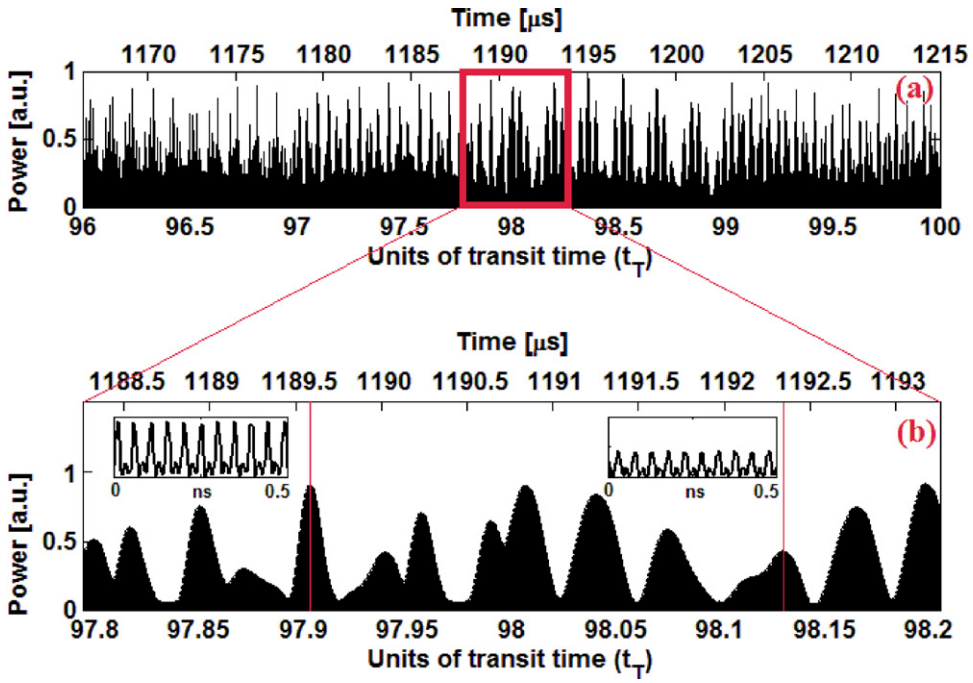

Figure 5. Calculated temporal interference signal power at the output of the dual-cavity configuration including a 2.5 km fiber spool (a) over 4 t_T, equal to ~50 μs. (b) Zoomed-in area in (a) over 0.4t_T, equal to ~5 μs. The insets in (b) show two 0.5 ns time-window showing interference signal powers centered at two different times.

roundtrip time are observed due to mode beating within each Stokes linewidth demonstrating an unstable behavior [32, 33]. Note that the time window (50 μs) observed here is much longer than a round-trip time in the cavity (~0.8 μs in this case).

In previous studies, limited information from RF spectrum analysis cannot lead to conclusive continuous single-mode operation [27, 28]. When long cavities are studied, an insufficient time span of less than a round-trip time is often used, which would limit the spectral resolution, thus not resolving the modes. Mode hopping due to environment perturbation was also observed by Stepanov and Cowle [19] which affects the MWBEFL output emission. This paper as well as Tang *et al's* [27] have shown momentarily single-mode operation in one spectrum with sufficient resolution for one round-trip, while stating that they observed mode-hopping over time. However, their results only show stable operation during ~10 μs, which is insufficient to qualify as a long term stable commercial laser source. Hence, a rigorous study of the laser stability needed to be undertaken on a longer time span. By doing so, we have observed such an instability. This instability leads to complications when an MWBEFL is used in intensity encoded schemes and would require additional referencing components to compensate for the fluctuations. Different pump powers (~100 mW–4 W), pumping configurations (single bi-directionnal EDFA, single directional EDFA in each cavity, lower gain EDFA, etc), and fiber lengths were tested during these experiments to try to find a stable solution, but without success. In this study, we have shown a few configurations which have been thoroughly analyzed. It could be possible that other configurations may show longer stability time of several tens of μs, allowing stable single-mode operation for a few round-trip periods before mode-hopping occurs. However, our experiments in such alternative configurations show that such mode instability always occurs given a long enough observation time window. Under very specific conditions, it may be that some long cavity MWBEFLs may be stable and operate single-mode, as seems to be shown by some previous works [27, 28], but those results are hardly reproducible and therefore not applicable to a commercial easy turn-key laser system, contrary to what has been claimed in the literature. An alternative configuration that could be further studied would be to use a quasi-cavity MWBEFL, where each Stokes is generated through a single pass. The counter-propagating nature of the SBS is then used as a 'cavity mirror' to amplify the generated Stokes and use it as the next pump [29]. Such a scheme has no cavity mode, therefore one could expect a more stable operation. Another solution would be to simply ensure that only one mode is excited per Stokes wave, such as recently proposed by Liu *et al* [41] where a single-mode MWBEFL using a very short length of fiber was demonstrated, and one which could prove to be stable in time.

The other effect from the presence of modes within the SBS bandwidth can be seen in the application of the MWBEFL as a pulsed laser source. From our results, phase-locking in a long cavity is not possible because the modes evolve with different phases and powers. Due to thermal fluctuation, modes drift from one round trip to another and different modes can become dominant. Therefore, no stable phase relationship can exist with such a long cavity

especially when more than one mode is present within the SBS gain bandwidth. Indeed, modes have different phase relationships, which result in destructive and constructive interference pattern necessary to generate a pulse train. The formation of stable pulse trains in long resonators seems unlikely due to the instabilities that have been observed. A solution to this is to ensure the existence of only one mode per SBS bandwidth. However, this limits the length of cavity to less than ~10 m. A system as demonstrated by Liu *et al* [41] could potentially have a stable phase which could lead to a proper pulse train. Even if the cavity is short and there is one mode under each Brillouin gain bandwidth, phase-locking is not guaranteed because of dispersive effects. FWM also affects a frequency comb generated through cSBS although the Stokes spacing is not equidistant by nature. When FWM is involved, Brillouin Stokes lines are pulled to the right spacing by phase-sensitive FWM gain and coherence between pump and Stokes waves can be achieved [3, 12, 13]. However, no strong FWM is seen in the results discussed in this paper, therefore there is no clear evidence of coherence between each Stokes wave.

6. Conclusion

We have shown both experimentally and theoretically the existence of intensity instability in hybrid SBS/EDFA multi-wavelength fiber lasers. When using an in-cavity EDFA combined with different types of fiber spools within the cavity as an SBS gain medium, a minimum length of several tens of meters is typically required. Such lengths will bring several cavity modes with different phases and powers within the SBS gain bandwidth, which are, we believe, the source of the MWBEFL's instability. In fact, these modes are already in a fragile stability regime due to SBS relaxation dynamics. Their competition and random hopping from one position to another from temperature fluctuations seems to worsen the SBS's chaotic behavior. Such instabilities make the use of the individual lines as a laser source for a transmission channel a problematic choice, especially for intensity encoded schemes for data transfer. As shown in our results, mode beating is indeed present as observed in the frequency domain when performing FFT of the temporal data. Although some configurations under specific conditions may offer some temporary stability, our typical results show that those conditions are not generally reproducible as necessary for commercial device applications. The temporal instability problem observed for individual lines and confirmed by simulation, remains an issue when a cSBS frequency comb is used as a phase locked self-pulsing source. This problem causes varying destructive and constructive interference and hence intensity fluctuations in the output pulses. Indeed, our results from measurement and numerical analysis demonstrate that the overall temporal characteristics for both configurations using different fibers suffer from unstable behavior and mode beating. Avoiding mode beating with a feedback mechanism could potentially be possible, but due to the long length of the cavity, mitigating the temperature and strain would be a hard task to perform. However, this kind of stabilization would be useless unless the excitation of all the cavity modes is suppressed as well. This can only be achieved by using a short cavity or an additional in-cavity mode filter.

Acknowledgments

This work was supported by the Australian Research Councils, Center of Excellence CUDOS (CE110001018) and Laureate Fellowship (FL120100029) schemes. RK acknowledges support from the Canada Research Chairs program and the Natural Sciences and Engineering Research Council of Canada's Discovery Grants program. VLI acknowledges support from NSERC PhD scholarship and the support from an FRQNT travel grant. SL acknowledges support from NSERC Vanier scholarship. This work was a collaboration between Eggleton's group (CUDOS, Sydney, Australia), and Kashyap's group (Fabulas laboratory, Montreal, Canada).

References

[1] Udem T, Holzwarth R and Hänsch T W 2002 Optical frequency metrology *Nature* **416** 233–7
[2] Holzwarth R, Udem T, Hänsch T W, Knight J, Wadsworth W and Russell P S J 2000 Optical frequency synthesizer for precision spectroscopy *Phys. Rev. Lett.* **85** 2264
[3] Braje D, Hollberg L and Diddams S 2009 Brillouin-enhanced hyperparametric generation of an optical frequency comb in a monolithic highly nonlinear fiber cavity pumped by a cw laser *Phys. Rev. Lett.* **102** 193902
[4] Li J, Lee H and Vahala K J 2013 Microwave synthesizer using an on-chip Brillouin oscillator *Nat. Commun.* **4**
[5] Al-Mansoori M, Abd-Rahman M K, Mahamd Adikan F and Mahdi M 2005 Widely tunable linear cavity multiwavelength Brillouin-erbium fiber lasers *Opt. Express* **13** 3471–6
[6] Brackett C A 1990 Dense wavelength division multiplexing networks: principles and applications *IEEE J. Sel. Areas Commun.* **8** 948–64
[7] Butler D L, Wey J S, Chbat M W, Burdge G L and Goldhar J 1995 Optical clock recovery from a data stream of an arbitrary bit rate by use of stimulated Brillouin scattering *Opt. Lett.* **20** 560–2
[8] Luo Z *et al* 2008 Stable and spacing-adjustable multiwavelength Raman fiber laser based on mixed-cascaded phosphosilicate fiber Raman linear cavity *Opt. Lett.* **33** 1602–4
[9] Kippenberg T J, Holzwarth R and Diddams S 2011 Microresonator-based optical frequency combs *Science* **332** 555–9

[10] Kawanishi T, Sakamoto T, Shinada S and Izutsu M 2004 Optical frequency comb generator using optical fiber loops with single-sideband modulation *IEICE Electron. Express* **1** 217–21
[11] Agrawal G P 2000 *Nonlinear Fiber Optics* (Berlin: Springer)
[12] Büttner T F *et al* 2014 Phase-locking and pulse generation in multi-frequency brillouin oscillator via four wave mixing *Sci. Rep.* **4** 2097
[13] Büttner T F *et al* 2014 Phase-locked, chip-based, cascaded stimulated Brillouin scattering *Optica* **1** 311–4
[14] Song Y, Zhan L, Ji J, Su Y, Ye Q and Xia Y 2005 Self-seeded multiwavelength Brillouin-erbium fiber laser *Opt. Lett.* **30** 486–8
[15] Liu Y-G, Dong X, Shum P, Yuan S, Kai G and Dong X 2006 Stable room-temperature multi-wavelength lasing realization in ordinary erbium-doped fiber loop lasers *Opt. Express* **14** 9293–8
[16] Nasir M M, Yusoff Z, Al-Mansoori M, Rashid H A and Choudhury P 2008 Broadly tunable multi-wavelength Brillouin-erbium fiber laser in a Fabry–Perot cavity *Laser Phys. Lett.* **5** 812
[17] Shahi S, Harun S and Ahmad H 2009 Multi-wavelength Brillouin fiber laser using Brillouin-Rayleigh scatterings in distributed Raman amplifier *Laser Phys. Lett.* **6** 737
[18] Hambali N A, Al-Mansoori M, Ajiya M, Bakar A, Hitam S and Mahdi M 2011 Multi-wavelength Brillouin-Raman ring-cavity fiber laser with 22 GHz spacing *Laser Phys.* **21** 1656–60
[19] Stepanov D Y and Cowle G J 1997 Properties of Brillouin/erbium fiber lasers *IEEE J. Sel. Top. Quantum Electron.* **3** 1049–57
[20] Kang M, Joly N and Russell P S J 2013 Passive mode-locking of fiber ring laser at the 337th harmonic using gigahertz acoustic core resonances *Opt. Lett.* **38** 561–3
[21] Nasir M M, Yusoff Z, Al-Mansoori M, Rashid H A and Choudhury P 2009 Low threshold and efficient multi-wavelength Brillouin-erbium fiber laser incorporating a fiber Bragg grating filter with intra-cavity pre-amplified Brillouin pump *Laser Phys. Lett.* **6** 54
[22] Song Y, Zhan L, Hu S, Ye Q and Xia Y 2004 Tunable multiwavelength Brillouin-erbium fiber laser with a polarization-maintaining fiber Sagnac loop filter *IEEE Photonics Technol. Lett.* **16** 2015–7
[23] Min B, Kim P and Park N 2001 Flat amplitude equal spacing 798-channel Rayleigh-assisted Brillouin/Raman multiwavelength comb generation in dispersion compensating fiber *IEEE Photonics Technol. Lett.* **13** 1352–4
[24] Tang J, Sun J, Chen T and Zhou Y 2011 A stable optical comb with double-Brillouin-frequency spacing assisted by multiple four-wave mixing processes *Opt. Fiber Technol.* **17** 608–11
[25] Shirazi M, Harun S and Ahmad H 2014 Multi-wavelength Brillouin Raman erbium-doped fiber laser generation in a linear cavity *J. Opt.* **16** 035203
[26] Liu Y-G, Wang D and Dong X 2008 Stable room-temperature multi-wavelength lasing oscillations in a Brillouin–Raman fiber ring laser *Opt. Commun.* **281** 5400–4
[27] Tang J, Sun J, Zhao L, Chen T, Huang T and Zhou Y 2011 Tunable multiwavelength generation based on Brillouin-erbium comb fiber laser assisted by multiple four-wave mixing processes *Opt. Express* **19** 14682–9
[28] Zhan L, Ji J, Xia J, Luo S and Xia Y 2006 160-line multiwavelength generation of linear-cavity self-seeded Brillouin-erbium fiber laser *Opt. Express* **14** 10233–8
[29] Ajiya M, Mahdi M A, Al-Mansoori M H, Hitam S and Mokhtar M 2009 Seamless tuning range based-on available gain bandwidth in multiwavelength Brillouin fiber laser *Opt. Express* **17** 5944–52
[30] Shee Y, Al-Mansoori M, Ismail A, Hitam S and Mahdi M 2011 Multiwavelength Brillouin-erbium fiber laser with double-Brillouin-frequency spacing *Opt. Express* **19** 1699–706
[31] Loranger S, Iezzi V L and Kashyap R 2012 Demonstration of an ultra-high frequency picosecond pulse generator using an SBS frequency comb and self phase-locking *Opt. Express* **20** 19455–62
[32] Lecoeuche V, Randoux S, Ségard B and Zemmouri J 1996 Dynamics of a Brillouin fiber ring laser: off-resonant case *Phys. Rev.* A **53** 2822
[33] Harrison R G, Ripley P M and Lu W 1994 Observation and characterization of deterministic chaos in stimulated Brillouin scattering with weak feedback *Phys. Rev.* A **49** R24
[34] Lecoeuche V, Randoux S, Segard B and Zemmouri J 1996 Dynamics of stimulated Brillouin scattering with feedback *Quantum Semiclass. Opt.: J. Eur. Opt. Soc.* B **8** 1109
[35] Ogusu K and Sakai A 2002 Generation and dynamics of cascaded stimulated Brillouin scattering in a high-finesse fiber Fabry–Pérot resonator *Japan. J. Appl. Phys.* **41** 609
[36] Boyd R W, Rzążewski K and Narum P 1990 Noise initiation of stimulated Brillouin scattering *Phys. Rev.* A **42** 5514
[37] Ghatak A and Thyagarajan K 1998 *An Introduction to Fiber Optics* (Cambridge: Cambridge University Press)
[38] Li H and Ogusu K 2000 Instability of stimulated Brillouin scattering in a fiber ring resonator *Opt. Rev.* **7** 303–8
[39] Bar-Joseph I, Friesem A, Lichtman E and Waarts R 1985 Steady and relaxation oscillations of stimulated Brillouin scattering in single-mode optical fibers *J. Opt. Soc. Am.* B **2** 1606–11
[40] Bar-Joseph I, Dienes A, Friesem A, Lichtman E, Waarts R and Yaffe H 1986 Spontaneous mode locking of single and multi mode pumped SBS fiber lasers *Opt. Commun.* **59** 296–8
[41] Liu J, Zhan L, Wang G, Xiao P, Zhang L and Shen Q 2014 Uniform amplitude multi-wavelength single-longitudinal-mode Brillouin–erbium fiber lasers *J. Mod. Opt.* **61** 969–72